Dynamics of the RING Domain from Human TRAF6 by ^{15}N NMR Spectroscopy: Implications for Biological Function†

Craig J. Markin, Linda F. Saltibus, and Leo Spyracopoulos*

Department of Biochemistry, University of Alberta, Edmonton, AB T6G 2H7, Canada

Received February 12, 2008; Revised Manuscript Received July 22, 2008

ABSTRACT: Activation of transcription factor NF-κB requires Lys63-linked polyubiquitination of the E3 ubiquitin ligase TRAF6 via protein−protein interactions mediated by a RING domain. In this study, intra- and intermolecular chemical exchange processes of the TRAF6 RING domain were analyzed by ^{15}N NMR spectroscopy. Micro- to millisecond time scale motions were assessed through R_1, R_2, NOE, and cross-correlated relaxation measurements, and the kinetics of these motions were quantified with relaxation dispersion. The relaxation experiments indicate that the protein core is rigid, consistent with the functional requirement that RING domains form a binding scaffold for E2 ubiquitin conjugation enzymes. Chemical exchange is observed at the C-terminal end of the main α-helix of the RING domain. The C-terminal end of the main α-helix from the RING domain is involved in E2−E3 interactions, and modulation of slow motions for this region of the helix may be a general mechanism by which these interactions achieve ubiquitin transfer. Chemical shift mapping indicates that the TRAF6 RING domain does not self-associate in solution. Numerous RING domains are homo- or heterodimeric, and this is thought to be a functional necessity for recruitment of substrates for ubiquitination, or recruitment of multiple E2 enzymes for efficient substrate ubiquitination. However, lack of self-association for the RING domain from TRAF6, and the observation that the intact protein is a trimer, suggests that close association of RING domains within a homodimeric scaffold may not be a fundamental requirement for biological function.

The TNF[1] receptor superfamily and the interleukin-1/Toll-like receptors utilize TRAF proteins as signaling adaptors (*1, 2*). These receptors recruit TRAF proteins and are involved in the activation of cells, cell differentiation, immunity, and signaling for survival (*3, 4*). The adaptor proteins TRAF2 and TRAF6 have been studied intensively due to their role in the activation of NF-κB (*5, 6*), a transcription factor that triggers genes involved in the cell cycle, differentiation, apoptosis, and the immune response (*7*).

The C-terminal regions of TRAF2 and TRAF6 are composed of a MATH domain that is responsible for interactions with the cytoplasmic domains from TNF receptors (*8*). The N-terminal region of TRAF6 is critical for signaling and contains a RING domain (*9, 10*). The RING domain from TRAF6 is believed to function as an E3 ubiquitin ligase and plays a role in autoubiquitination by catalyzing covalent attachment of Lys63 poly-Ub chains, through interaction with the E2 Ubc13 (*11, 12*). The first step of the autoubiquitination process involves attachment of a single Ub to TRAF6 and occurs with slow kinetics (*13*), consistent with the weak binding observed between the RING domain and Ubc13 (*10*). In addition, the RING domain from TRAF6 has been found to be important in autodegradation and the induction of apoptosis (*14*). These studies underscore the fact that the processes underlying substrate ubiquitination and subsequent chain elongation are currently not clearly understood (*15*).

RING domains from E3 ubiquitin ligases carry out their biological functions by binding their cognate E2 ubiquitin conjugation enzymes, as typified by the structure of c-Cbl bound to UbcH7 (*16*). It has been noted (*17, 18*) that many E3 ligases homo- or heterodimerize directly through their RING or RING-like domains to achieve their biological function (*19, 20*). For example, it is believed that the RING−RING heterodimer is essential for substrate recruitment and efficient ubiquitin transfer for the Bmi-1-RING1B polycomb group ubiquitin ligase complex (*20*).

In this study, the E3 ubiquitin ligase RING domain from TRAF6 (residues 67−124) was determined to be monomeric in solution, through analysis of $^{1}H-^{15}N$ two-dimensional (2D) NMR spectra with changes in protein concentration. Furthermore, chemical exchange phenomena on the micro- to millisecond time scale were assessed qualitatively using model-free analysis of ^{15}N R_1, ^{15}N R_2, and $\{^{1}H^{N}\}-^{15}N$ NOE and measurement of η_{xy} and η_z cross-correlated relaxation

† This work was supported by grants from the Canadian Institutes of Health Research (CIHR) and the Alberta Heritage Foundation for Medical Research (AHFMR). L.S. is an AHFMR Senior Scholar.

* To whom correspondence should be addressed. E-mail: leo.spyracopoulos@ualberta.ca. Phone: (780) 492-2417. Fax: (780) 492-0886.

[1] Abbreviations: AIC, Akaike's Information Criteria; CPMG, Carr−Purcell−Meiboom−Gill; DSS, 2,2-dimethyl-2-silapentane-5-sulfonate; E2, ubiquitin-conjugating enzyme; E3, ubiquitin protein ligase; HSQC, heteronuclear single-quantum coherence; INEPT, insensitive nuclei enhanced by polarization transfer; MATH domain, merpin and TRAF homology domain; NMR, nuclear magnetic resonance; NOE, nuclear Overhauser effect; RING, really interesting new gene; rmsd, root-mean-square deviation; R_1, longitudinal relaxation rate; R_2, transverse relaxation rate; TNF, tumor necrosis factor; TRAF, tumor necrosis receptor-associated factor; TRAF6-RD, TRAF6-RING domain; Ub, ubiquitin; η_{xy} and η_z, transverse and longitudinal cross-correlated relaxation rate constants, respectively.

10.1021/bi800252x CCC: $40.75
Published on Web 08/30/2008

rates and analyzed quantitatively using CPMG relaxation dispersion measurements (*21*−*23*). The relaxation dispersion experiments were interpreted in a simple fashion by assuming chemical exchange between two sites. For residues near the C-terminal end of the main α-helix within TRAF6-RD, chemical exchange phenomena were rationalized by predicting ^{15}N chemical shifts for the ensemble of 50 solution structures for TRAF6-RD (2JMD) (*10*) with SHIFTS (*24*−*26*).

MATERIALS AND METHODS

Purification of [U-^{15}N]TRAF6-RD. Overexpression and purification of ^{15}N-labeled TRAF6-RD were carried out as previously described (*10*), with the exception that LB and M9 minimal media were supplemented with 100 μM $ZnCl_2$ and 50 mM TRIS or BIS-TRIS, 150 mM NaCl, pH 7.0 buffer was used for cell lysis and subsequent protein purification.

^{15}N Chemical Shift Mapping. NMR samples contained 600 μL of a 95:5 H_2O/D_2O mixture, containing 50 mM TRIS, 150 mM NaCl (pH 7.0), and 0.14 mM DSS as a chemical shift reference with protein concentrations of 0.304, 0.149, 0.110, 0.069, and 0.030 mM TRAF6-RD in 5 mm standard NMR tubes. In addition, as a control, a 10-fold dilution of ∼0.5 mM TRAF6-RD in the absence of DSS was conducted using similar conditions. For chemical shift mapping and ^{15}N R_2 measurements in the presence of DSS, NMR spectra were recorded at 25 °C using a Varian Unity INOVA 600 MHz NMR spectrometer and the sensitivity-enhanced, 2D ^{1}H−^{15}N HSQC experiment for measurement of ^{15}N R_2 (*21*). Spectra were collected with relaxation delays of 10 and 90 ms at each protein concentration. Chemical shift mapping was conducted using spectra acquired with the 10 ms delay. ^{15}N R_2 values were calculated from the natural logarithm of the ratio of cross-peak intensities at 10 and 90 ms divided by 80 ms. Protein concentrations were determined by quantitative amino acid analysis (*27*). The error in protein concentration was estimated to be ∼5%, on the basis of previous concentration determinations for the protein troponin C, conducted in triplicate (*28*). The number of transients collected was 16, 32, 32, 40, and 60 for protein concentrations of 0.304, 0.149, 0.110, 0.069, and 0.030 mM, respectively.

Spectra were processed using NMRPipe (*29*), and chemical shift assignments for cross-peaks within the 2D ^{1}H−^{15}N HSQC NMR spectra were made with Sparky (*30*), and previously published chemical shifts for TRAF6-RD (BRMB accession number 15014) (*10*). Although the chemical shifts for residues K104 and F118 were unambiguous for the chemical shift mapping experiments, they became overlapped slowly over the course of a few days and could not be unambiguously assigned for the cross-correlated relaxation experiments and model-free analysis described in subsequent sections.

^{15}N chemical shift mapping was accomplished by following changes in 2D ^{1}H−^{15}N HSQC spectra upon dilution. These changes upon dilution occur only in the presence of DSS and therefore reflect binding of DSS to TRAF6. Thus, per residue plots of ^{15}N chemical shift (δ_{obs}) as a function of the protein:DSS ratio were fit to a 1:1 protein−ligand binding equilibrium to extract K_D, δ_{free}, and δ_{bound}. The precision of the chemical shift measurement (0.001 and 0.002 ppm for the $^1H^N$ and ^{15}N dimensions, respectively) was determined by taking the mean standard deviation over all assigned residues from five separate samples of [*U*-^{15}N]-ubiquitin at concentrations ranging from 0.2 to 1.5 mM, using acquisition parameters similar to those used for TRAF6-RD.

The average ^{15}N R_2 values and their average errors as a function of increasing protein concentration are 5.9 ± 0.7, 5.7 ± 0.4, 6.1 ± 0.4, 6.3 ± 0.3, and 7.2 ± 0.4 s^{-1}. The increase in the average ^{15}N R_2 values as a function of protein concentration indicates that the underlying equilibrium may be more complicated than 1:1 protein−DSS binding.

^{15}N R_2 Constant-Time, Relaxation-Compensated CPMG Dispersion Measurements. ^{15}N constant-time, relaxation-compensated CPMG dispersion experiments (*23, 31*) were carried out at 600 and 800 MHz with a 350 μL sample of 0.43 mM TRAF6-RD in a 95:5 H_2O/D_2O mixture, containing 50 mM BIS-TRIS, 150 mM NaCl, 5 mM DTT, 100 μM zinc sulfate (pH 7.0), and 0.14 mM DSS as an internal chemical shift reference, in a 5 mm Shigemi microcell NMR tube. The gNcpmgex_NH sequence from the Varian Biopack suite of pulse sequences was employed at 600 and 800 MHz. For the ^{15}N CPMG pulse trains, the ^{15}N 90° pulse widths were 44 and 54 μs at 600 and 800 MHz, respectively, and the constant relaxation time was 40 ms. The 800 MHz spectrometer was equipped with a cryogenically cooled probe, and heating compensation (as implemented in the gNcpmgex_NH sequence) was required to maintain constant heating for all CPMG pulse repetition rates. Per residue $R_{2,eff}$ values were calculated according to eq 1 in ref *32*. $R_{2,eff}$ dispersion profiles at both magnetic field strengths were globally fit (*33*) to eq 25 (Carver−Richards equation) and eq 28 (fast exchange only) in ref *34* for individual residues using *Mathematica*, and AIC was used to discriminate between the two functions. Errors in the fitted parameters were obtained using Monte Carlo analyses for global fits. To obtain a qualitative structural interpretation of the dispersion measurements, main chain amide chemical shifts were predicted using the ensemble of 50 NMR solution structures for TRAF6-RD and SHIFTS (version 4.2) (*24*−*26*). Predicted ^{15}N $\Delta\omega$ values were taken to be the width of the per residue calculated chemical shift distributions at 1σ, except for F89, for which the distribution was trimmed by removing two predicted shifts with values ∼122 ppm from the main ensemble of predicted shifts whose values ranged from 113 to 117 ppm.

^{15}N R_1, ^{15}N R_2, {^{1}H}−^{15}N NOE, η_{xy}, and η_z Cross-Correlated Relaxation Measurements and Model-Free Analyses. Main chain amide ^{15}N η_{xy} and η_z rates were measured using sensitivity-enhanced 2D ^{1}H−^{15}N HSQC NMR experiments (*22*), at 600 MHz with pulse sequences coded in-house. Experiments were carried out with a 350 μL sample of ∼0.4 mM TRAF6-RD in a 95:5 H_2O/D_2O mixture containing 50 mM TRIS, 150 mM NaCl (pH 7.0), and 0.14 mM DSS as an internal chemical shift reference, in a 5 mm Shigemi microcell NMR tube. The per residue η_{xy} and η_z values were subsequently used with measurements of ^{15}N R_1, ^{15}N R_2, and {^{1}H}−^{15}N NOE (vide infra) to calculate per residue $R_{2,0}$ values; these were used to estimate an R_{ex} value (*22*). Errors were propagated accordingly from the spectral noise. R_{ex} values exceeding the mean by one standard deviation were considered significant. ^{15}N R_1, ^{15}N R_2, and {^{1}H}−^{15}N NOE experiments were conducted at 600 and 800 MHz using pulse sequences described in ref *21*, and with the same protein

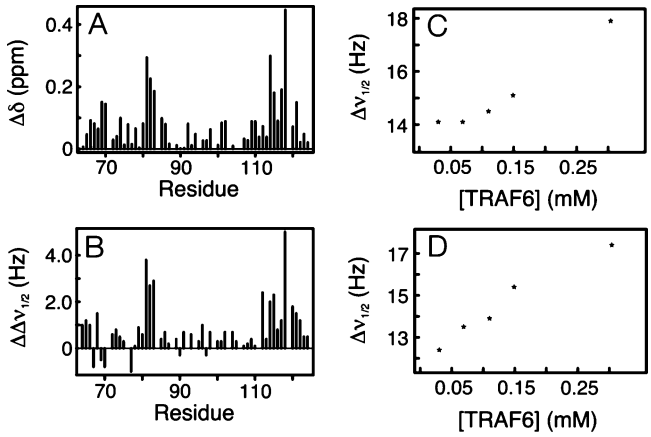

FIGURE 1: (A) Main chain amide ^{15}N chemical shift changes [$\Delta\delta = |\delta(\text{protein:DSS} = 0.2) - \delta(\text{protein:DSS} = 2.2)|$] for TRAF6-RD upon DSS binding. (B) Main chain amide ^{15}N line width changes [$\Delta\Delta\nu_{1/2} = \Delta\nu_{1/2}(\text{protein:DSS} = 2.2) - \Delta\nu_{1/2}(\text{protein:DSS} = 0.2)$] for TRAF6-RD upon dilution. (C) Concentration dependence of line widths for TRAF6-RD V81 in the presence of 0.14 mM DSS. (D) Concentration dependence of line widths for TRAF6-RD F118 in the presence of 0.14 mM DSS.

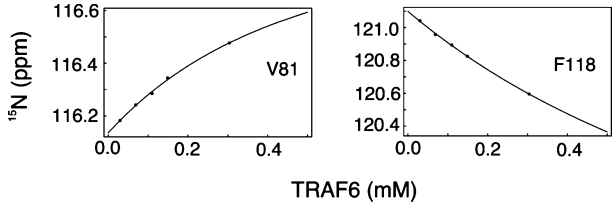

FIGURE 2: Main chain amide ^{15}N chemical shift changes for TRAF6-RD upon dilution, in the presence of 0.14 mM DSS.

sample that was used for measurements of η_{xy} and η_z cross-correlated relaxation rates. Per residue ^{15}N R_1, ^{15}N R_2, and $\{^1\text{H}\}-^{15}$N NOE values at 600 and 800 MHz were simultaneously subjected to a model-free analysis as previously described (*35*) using *Mathematica* (*36*), with model selection using AIC (*37*). For model-free analyses, a disadvantage of AIC compared to hypothesis testing using α values is that AIC always discriminates between models, whereas hypothesis testing can reveal whether different models are indistinguishable (*38*). For the model-free analysis, protein tumbling was assumed to be isotropic, with an overall correlation time of 4.17 ns, determined from the R_2/R_1 ratio.

RESULTS

^{15}N and $^1H^N$ NMR Chemical Shift and Line Width Perturbations upon Dilution. Line shape perturbations for TRAF6-RD upon dilution from 304 to 30 μM occur only in the presence of DSS and are summarized in Figure 1. The largest main chain amide ^{15}N chemical shift changes ($\Delta\delta$) exceed the mean by 1.5σ and are observed for residues V81, Q82, E114, and F118. The largest changes in line width ($\Delta\Delta\nu_{1/2}$), exceeding the mean line width change by 1.5σ, occur for residues V81 (Figure 1C), Q82, T83, and F118 (Figure 1D).

Chemical shift changes in 2D ^{1}H$-^{15}$N NMR spectra upon dilution for residues V81 and F118 from TRAF6-RD are shown in Figure 2. It should be noted that these changes occur only in the presence of DSS and, in the simplest interpretation, reflect 1:1 protein−DSS binding. ^{15}N $\Delta\delta$ values for V81 and F118 were fit to a 1:1 protein−DSS binding equilibrium to yield K_D values of 0.4 ± 0.2 and 1.0 ± 0.4 mM, respectively. In addition, changes in the ^{1}H chemical shift from the methyl groups of DSS upon protein dilution were also fit to a 1:1 protein−DSS binding equilibrium to yield a similar K_D of 0.2 ± 0.1 mM. Thus, for an average K_D of 0.5 mM, the fraction of free protein is ∼0.9 at a DSS concentration of 0.14 mM and a protein concentration of 0.4 mM.

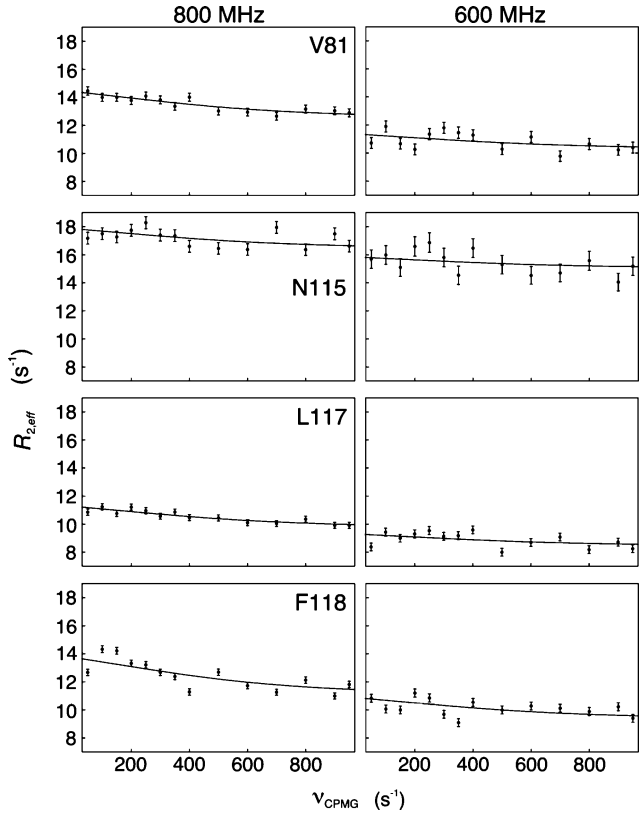

FIGURE 3: ^{15}N R_2 relaxation dispersion for TRAF6-RD, with multiple field data for each residue globally fit to chemical exchange between two sites, and k_{ex} fit globally for all residues.

^{15}N NMR R_2 Relaxation Dispersion. ^{15}N relaxation dispersion experiments were used to quantify chemical exchange processes on the micro- to millisecond time scale (Figures 3−5 and Tables 1 and 2). Residues V81, N115, L117, and F118 show line shape changes upon dilution (and concomitant increases in protein:DSS ratio), display dispersion curves that are characteristic of the fast exchange limit, and fit with a global k_{ex} of 3514 ± 620 s^{-1} (Figure 3 and Table 1). While residue T83 also displays line shape changes upon dilution, dispersion data for this residue were statistically better fit with the Carver−Richards equation (*39*) and had fitted parameters for chemical exchange similar to those for residues G86 and H87; these residues participate with T83 in an extensive hydrogen bonding network. Thus, residues T83, G86, and H87 were globally fit with the Carver−Richards equation with global p_a and k_{ex} values of 0.989 ± 0.004 and 532 ± 165 s^{-1}, respectively (Figure 4 and Table 2). Residues I98, R99, and D100 at the C-terminal end of the short α-helix in TRAF6-RD also display exchange with k_{ex} values of 1121 ± 123, 4690 ± 680, and 3569 ± 834 s^{-1}, respectively (Figure 5 and Table 1). The relaxation dispersion profile for residue K104 was fit with the Carver−Richards equation with a $\Delta\omega_N$ of 1213 ± 138 rad s^{-1} at 800 MHz (∼2 ppm) and with p_a and k_{ex} values of 0.98 ± 0.01 and 255 ± 264 s^{-1}, respectively (Figure 5). Finally, residues E110 and L112 display relax-

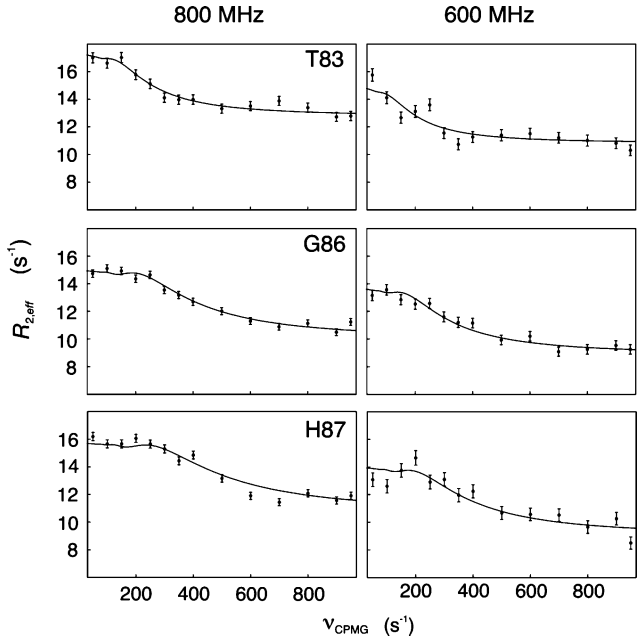

FIGURE 4: ^{15}N R_2 relaxation dispersion for TRAF6-RD, with multiple field data for each residue globally fit to chemical exchange between two sites, and parameters k_{ex} and p_a fit globally for all residues.

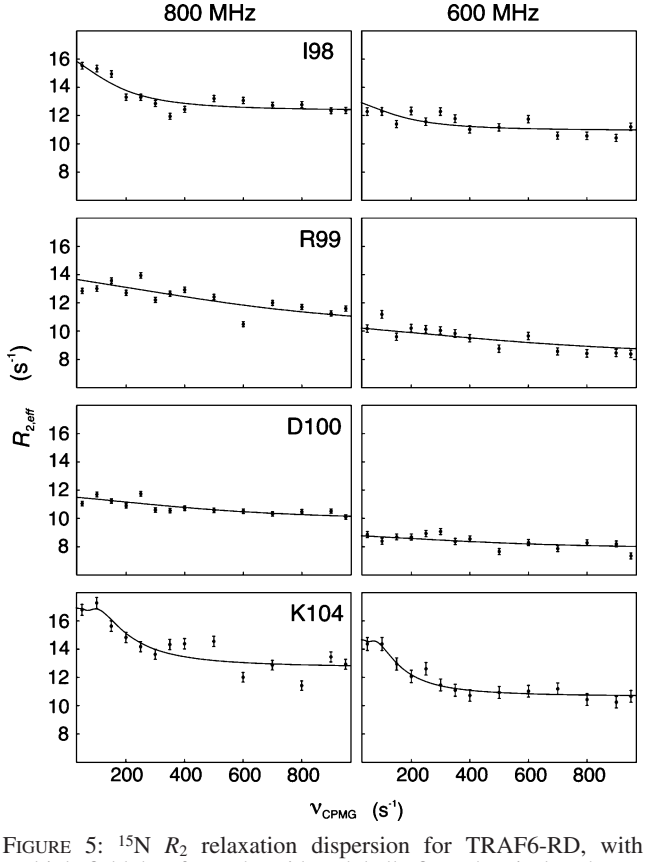

FIGURE 5: ^{15}N R_2 relaxation dispersion for TRAF6-RD, with multiple field data for each residue globally fit to chemical exchange between two sites, and individual residues analyzed separately.

ation dispersion with k_{ex} values of 2312 ± 629 and 6137 ± 2239 s^{-1}, respectively (Table 1).

^{15}N NMR Cross-Correlated Relaxation and Model-Free Analysis. Chemical/conformational exchange phenomena were further verified using ^{15}N cross-correlated relaxation measurements (Table 3). Residues 81−83, 86, 98, and 104/118 display R_{ex} terms that exceed the mean R_{ex} by 1σ. However, the calculated R_{ex} values for residues Q82 and I98 do not exceed 1σ within error. A model-free analysis was also performed using ^{15}N R_1, ^{15}N R_2, and {$^1H^N$}−^{15}N NOE data collected at 600 and 800 MHz, with the chief purpose of identifying residues undergoing chemical exchange. Residues 81−83, 86, 87, 98, 99, 104/118, 110, and 114 require R_{ex}^{600} terms ranging from ∼1 to 3 s^{-1} to fit their relaxation data (Table 4). Although model 4 (S^2, τ_e, R_{ex}) was chosen by AIC for residue 98, the S^2 value was unrealistic (0.07 ± 0.06), considering it is flanked by two residues with S^2 values of ∼0.83 and is found in a region of relatively well-defined structure. Thus, the model with the next lowest AIC value was chosen [model 3 (S^2, R_{ex})].

Table 1: Chemical Exchange Parameters for ^{15}N CPMG R_2 Dispersion of TRAF6-RD

residue[a]	$p_a p_b \Delta\omega^2$ (rad^2 s^{-2})[b]	$R_{2,0}$ (s^{-1})[b]	$R_{2,0}$ (s^{-1})[c]
V81	7190 ± 2154	12.4 ± 0.3	10.2 ± 0.2
I98	4434 ± 414	12.3 ± 0.1	10.9 ± 0.1
R99	18325 ± 4715	9.9 ± 0.4	8.1 ± 0.2
D100	6367 ± 2090	9.8 ± 0.2	7.8 ± 0.1
E110	10984 ± 3466	10.3 ± 0.4	9.4 ± 0.2
L112	39361 ± 30030	9 ± 2	9 ± 1
N115	5396 ± 2647	16.3 ± 0.4	15.0 ± 0.3
L117	5761 ± 1845	9.6 ± 0.2	8.4 ± 0.1
F118	10143 ± 2526	10.9 ± 0.3	9.2 ± 0.2

[a] Residues 81, 115, 117, and 118 were fit simultaneously (k_{ex} = 3514 ± 620 s^{-1}), and residues 98−100, 110, and 112 were fit individually (for k_{ex} values, see Results). [b] Data collected at 800 MHz. [c] Data collected at 600 MHz.

Table 2: Chemical Exchange Parameters for ^{15}N CPMG R_2 Dispersion of TRAF6-RD

residue[a]	$\Delta\omega$ (rad s^{-1})[b]	$R_{2,0}$ (s^{-1})[b]	$R_{2,0}$ (s^{-1})[c]
T83	1378 ± 167	12.8 ± 0.4	10.8 ± 0.2
G86	2375 ± 481	10.0 ± 0.9	8.9 ± 0.5
H87	2941 ± 420	10.7 ± 0.8	9.0 ± 0.4

[a] Simultaneous fits of the data yield a k_{ex} of 523 ± 165 s^{-1} and a p_a of 0.990 ± 0.004. [b] Data collected at 800 MHz. [c] Data collected at 600 MHz.

Table 3: Chemical Exchange Parameters from ^{15}N Cross-Correlated Relaxation Rates

residue	R_{ex}^{600} (s^{-1})	residue	R_{ex}^{600} (s^{-1})
V81	3.0 ± 0.3	G86	2.5 ± 0.6
Q82	2.0 ± 0.3	I98	1.9 ± 0.8
T83	3.1 ± 0.4	K104/F118[a]	2.9 ± 0.2

[a] K104 and F118 were overlapped for these experiments.

Table 4: Chemical Exchange Parameters from ^{15}N Model-Free Analysis

residue	R_{ex}^{600} (s^{-1})[a]	residue	R_{ex}^{600} (s^{-1})[a]
V81	1.1 ± 0.1	I98	1.6 ± 0.1
Q82	0.7 ± 0.2	R99	0.8 ± 0.1
T83	1.6 ± 0.1	K104/F118[b]	1.6 ± 0.1
G86	2.1 ± 0.2	E114	0.7 ± 0.2
H87	3.1 ± 0.1		

[a] Only R_{ex} values of >0.6 s^{-1} are reported. [b] K104 and F118 were overlapped for these experiments.

DISCUSSION

Characterization of TRAF6-RD Self-Association and DSS Binding Using Chemical Shift Mapping. In this study, we utilized an array of ^{15}N NMR spectroscopic approaches to

assess intra- and intermolecular chemical exchange processes for the main chain of the TRAF6 RING domain. For line shape changes upon protein dilution in the presence of DSS, large ^{15}N $\Delta\delta$ and $\Delta\Delta\nu_{1/2}$ values are indicative of structural changes accompanying self-association. However, chemical shift changes upon 10-fold dilution of ~0.5 mM TRAF6-RD are not observed in the absence of DSS. This result indicates that TRAF6-RD is monomeric in solution but associates with DSS, a common chemical shift reference standard (*40*) that is an anionic detergent. Interestingly, line width increases for residues V81 and F118 in the ^{15}N dimension are observed with increasing protein concentration and the concomitant increase in protein:ligand ratio (Figure 1C,D). For fast chemical exchange, line widths are expected to decrease for a 1:1 protein−ligand interaction with an increase in protein:ligand ratio, whereas the opposite effect is observed for TRAF6-RD−DSS binding. Therefore, it is likely that the underlying equilibrium is more complex than 1:1 protein−DSS binding.

Characterization of TRAF6-RD Chemical Exchange Processes Using Relaxation Dispersion, Model-Free Analysis, and Cross-Correlated Relaxation Measurements. A key issue in the interpretation of relaxation dispersion measurements is the correct attribution of chemical exchange to intra- or intermolecular processes. For example, intramolecular instability for a ubiquitin-associated domain was characterized in terms of a folding−unfolding equilibrium (*41*). Dispersion experiments conducted at multiple ligand concentrations have been used successfully to separate intra- and intermolecular exchange processes for titration of the regulatory subunit of protein kinase A with cAMP (*42*), and titration of the phosphorylated kinase inducible activation domain of CREB with the KIX domain from CREB binding protein (*43*). The kinetics of the monomer−dimer equilibrium for the dimeric four-helix bundle α_2D have been quantified using ^{13}C relaxation dispersion spectroscopy (*44*), and monomer−dimer exchange for the protein $GB1^{A34F}$ was characterized recently using ^{15}N relaxation dispersion in combination with analysis of 2D $^{1}H-^{15}N$ NMR spectral changes upon dilution (*45*).

For the relaxation dispersion of TRAF6-RD, residues V81, N115, L117, and F118 were observed to undergo fast chemical exchange (Figure 3 and Table 1). Although only the product $p_a p_b \Delta\omega_N^2$ can be determined from curve fitting, if we assume $p_a = 0.9$ and $p_b = 0.1$ (corresponding to the fractions of free and DSS bound protein with a K_D of 0.5 mM and TRAF6 and DSS concentrations of 0.4 and 0.14 mM, respectively), the fitted values of $p_a p_b \Delta\omega_N^2$ at 800 MHz give rise to maximum $\Delta\omega_N$ values ranging from ~180 to 250 rad s^{-1} (from ~0.5 to 0.7 ppm). In the presence of DSS, these residues undergo ^{15}N chemical shift changes upon dilution, raising the possibility that the kinetics associated with DSS−protein binding may be the source of chemical exchange. However, these maximum $\Delta\omega_N$ values are ~10-fold too small if structural changes in the protein accompany DSS binding. In addition, the increase in protein line widths with an increase in protein:DSS ratio (line width decreases are expected) is not consistent with 1:1 protein−DSS binding. These observations suggest that the interaction between protein and DSS is more complicated than 1:1 binding. Given that TRAF6 is a cytoplasmic signaling adaptor protein, DSS binding is not likely to be biologically significant, and a more detailed characterization of DSS binding kinetics is not warranted.

Residues I98, R99, and D100 are found near the C-terminus of the main α-helix in TRAF6-RD. These residues do not exhibit significant chemical shift changes upon dilution. Therefore, it is likely that the observed relaxation dispersion is due to intramolecular chemical exchange. We hypothesize that these residues are undergoing constrained helical fraying, potentially due to the fact that main chain hydrogen bonds near helical termini are not fulfilled. Motions for α-helices that are not constrained at their N- or C-termini typically occur on the nano- to picosecond time scale (*46*). For TRAF6-RD, the N- and C-termini of the main α-helix are constrained, in the sense that the polypeptide chain participates in additional tertiary structural interactions beyond the termini, and these may serve to slow the typical pico- to nanosecond time scale of motion for unconstrained termini of α-helices to the micro- to millisecond time scale. If we assume that the distribution of structures observed in the NMR ensemble (2JMD) at or near the ends of the main α-helix is a reasonable representation of conformational states between which transitions can occur, the ^{15}N $\Delta\omega$ values predicted by SHIFTS are 1.48, 1.03, and 1.95 ppm for residues 98−100, respectively; these residues are found at the C-terminal end of the α-helix (relaxation dispersion was not detected at the N-terminal end of the helix). In comparison, residues I94 and I95 are located in the middle of the helix and have buried side chains, and the predicted widths of the chemical shift distributions are 0.63 and 0.64 ppm, respectively. Additionally, these residues do not exhibit relaxation dispersion. Residues K96 and S97 are also near the middle of the helix and do not show relaxation dispersion but display larger widths for their predicted chemical shift distributions of 1.01 and 2.38 ppm, respectively. However, the larger widths for these residues arise mainly from contributions to the ^{15}N amide chemical shift due to the conformation of exposed side chains and are likely to be averaged to smaller values by fast time scale side chain fluctuations. In addition, the width of the predicted ^{15}N chemical shift distribution for residue F89 has a smaller value of 0.71 ppm. This residue packs within the hydrophobic core against residue I94 and does not display relaxation dispersion.

It should be noted that on the basis of the SHIFTS predictions, constrained helical fraying can potentially give rise to relaxation dispersion for residues at the N-terminal end of the α-helix, but this was not observed. A more fundamental analysis of the time scale and nature of chemical exchange processes potentially associated with constrained helical fraying can be obtained using molecular dynamics simulations, combined with quantum mechanical or empirical chemical shift calculations (*26*). However, these simulations are beyond the scope of this study, and the time scale necessary to observe micro- to millisecond time scale fluctuations is computationally intractable.

Finally, we note that for residues 98−100, the widths of their chemical shift distributions exceed the maximum $\Delta\omega$ values from the relaxation dispersion experiments by ~4-fold (0.3−0.5 ppm). This observation suggests that a two-state transition is not appropriate if the underlying chemical exchange process is helix-fraying. Additionally, it is possible that the exchange processes observed at the C-terminal end

of the α-helix reflect conformational transitions of His103, as observed in relaxation dispersion studies of the protein plastocyanin (*47*). The main chain amide resonance for this residue is not observed in 2D $^{1}H-^{15}N$ NMR spectra, presumably due to line broadening, and the adjacent residue K104 undergoes conformational exchange (Figure 5).

For residues T83, G86, and H87, our straightforward structure-based analysis does not provide meaningful insights into the underlying chemical exchange process. These residues participate in an extensive hydrogen bond network involving H-bond donors and acceptors from both the side chain and main chain. The relaxation dispersion may be the result of chemical exchange processes resulting from zinc binding, given that the side chain from H87 is believed to coordinate Zn^{2+}. However, Zn^{2+} binding to the BRCA1 RING domain occurs with high affinity (*48*), and metal exchange for the RING domain from CNOT4 occurs with slow kinetics (*49*) consistent with the relaxation dispersion experiments. The kinetics of Zn^{2+} binding for TRAF6-RD would need to be quantified to identify the origin of chemical exchange for residues T83, G86, and H87. Regardless of the source of chemical exchange, intra- or intermolecular modulation of the H-bond network in which residues T83, G86, and H87 participate is a likely source for their observed relaxation dispersion.

The remaining residues that display relaxation dispersion (K104, E110, and L112) are found proximal to loop L2 (residues 105−108) that is involved in coordinating zinc. Residue K104 is found in an isolated β-bridge, and residues E110 and L112 are not involved in regular secondary structure, as determined using DSSP (*50*). These residues do not display chemical shift changes upon dilution, and it is not obvious how their motions may be coupled to zinc binding; thus, the relaxation dispersion results may simply reflect intramolecular main chain dynamics.

In this study, ^{15}N R_1, ^{15}N R_2, $\{^{1}H^{N}\}-^{15}N$ NOE, and η_{xy} NMR relaxation measurements were used to qualitatively identify residues undergoing chemical exchange. All residues (except Q82) that display R_{ex} terms, as established from cross-correlated relaxation rate measurements, also display ^{15}N relaxation dispersion profiles indicative of chemical exchange. Residues V81, Q82, T83, and F118 display significant line shape perturbations upon dilution and concomitant changes in the protein:DSS ratio, and the R_{ex} values for these residues may reflect DSS binding, as discussed below in further detail for the model-free analysis. The observation of significant R_{ex} values for residues T83, G86, and H87 is consistent with the results from the relaxation dispersion experiments.

We previously conducted a model-free analysis for TRAF6-RD using data collected at 600 MHz (*10*). In this study, our goal was to identify residues requiring R_{ex} terms to fit their relaxation data, and we have the advantage that data collected at 600 and 800 MHz were simultaneously analyzed, thereby improving model selection, and taking the field dependence of R_{ex} into account. Herein, we have assumed quadratic field dependence for the model-free analysis, whereas for slow and intermediate exchange, this field dependence is not necessarily quadratic (*51*). From the relaxation dispersion analyses, all residues except T83, G86, H87, and K104 were fit with the relaxation dispersion equation for fast exchange only. Residues T83, G86, H87, and K104 were fit with the Carver−Richards equation, and the values of $k_{ex}/\Delta\omega$ and α range from 0.2 to 0.5 and from 0.1 to 0.4, respectively, indicating that these residues are in the slow exchange regime. For the model-free analysis, and analysis of cross-correlated relaxation rates, chemical exchange due to DSS binding can potentially contribute to the observed R_{ex} terms for residues 81−83 and 118 (Table 4). For example, we estimate the magnitude of observable R_{ex} terms to be ∼1 and 2 Hz at 600 and 800 MHz, respectively, given the experimental conditions used to acquire ^{15}N R_2, and assuming a rate of exchange of 2000 s^{-1}, with a p_a of 0.9 and a $\Delta\omega$ of 0.5 ppm. Thus, with the exception of residue Q82, these qualitative results agree with those from the relaxation dispersion experiments. However, we must consider that rotational diffusion anisotropy can potentially contribute to R_{ex} terms determined from cross-correlated relaxation measurements and model-free analysis (*22, 52*). In this study, anisotropic rotational diffusion does not substantially contribute to R_2 for residues 81−83 and 118. For example, for a protein with an isotropic overall correlation time of ∼4 ns, an axially symmetric rotational diffusion anisotropy of >2 is necessary for a maximum contribution of ∼2 s^{-1} to R_2, whereas monomeric TRAF6-RD is essentially spherical in shape, and monomeric using the solution conditions employed for relaxation measurements.

Biological Implications for Lack of TRAF6-RD Self-Association. Currently, it is not clear if E3 RING homo- or heteroassociation serves a general biological purpose (*18*). It has been observed that RING self-association creates supramolecular structures in vitro and these serve as polyvalent binding surfaces to provide a platform for multiple partner proteins (*53*). However, it is not certain if supramolecular structures are necessary for the activity of TRAF proteins, whose main function is to serve as cytoplasmic signaling adaptor proteins. For example, the C-terminal region of TRAF6, which does not contain the RING domain, is known to self-associate as a trimer (*54*), and this property is necessary for receptor binding (*55*). That is, the TNF receptor family is believed to be an example for the general theme of receptor activation through oligomerization, as the TNF receptor must associate as a trimer for activity (*56*). However, several RING domains are known to associate as homodimers or heterodimers (*17, 19, 57, 58*), and this property may be critical for biological function. For example, it has been suggested that molecular architectures of E3 ligases are tuned to orient and align E2 enzymes and substrates for efficient ubiquitin transfer, but it is not clear what role RING domain dimerization plays in this function (*17*). Although it is reasonable to expect that the regions surrounding RING domains are critical for dimerization, the isolated RING domain from Hdm2 was shown to form a homodimer at low concentrations and interact tightly with a RING domain from the homologue HdmX (*58*). It is interesting to note that the TRAF6 RING domain and surrounding regions are most similar in sequence to the corresponding region in the dimerization domain of RAG1, which contains a RING domain and a C2H2 zinc finger (*12, 59*). In the RAG1 dimer structure, the RING domains are not in physical contact, separated by ∼15 Å.

The lack of self-association of the RING domain from TRAF6 and the fact that the intact protein is a trimer suggest that the RING domains may not be closely associated in the

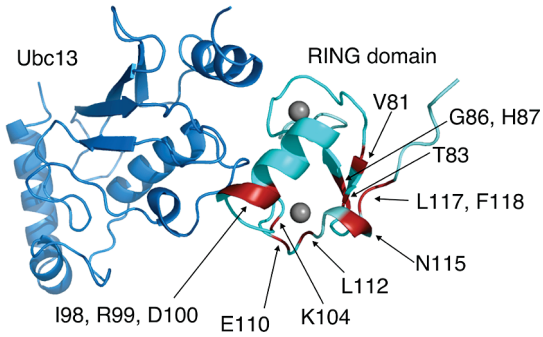

FIGURE 6: Superposition of TRAF6-RD and the E2 enzyme Ubc13 on the c-Cbl RING domain−UbcH7 complex (PDB entry 1FBV). Main chain atoms shown in the cartoon representation and residues displaying dispersion for main chain amide ^{15}N R_2 relaxation rates are colored red.

intact protein. With respect to functional significance, others have noted that a possible role for RING domains is to serve as protein−protein interaction modules involved in binding RING domains from different proteins (*58*). Therefore, maintaining the RING domains physically separated in intact TRAF6 may help fulfill this purpose.

Biological Implications of TRAF6-RD Slow Time Scale Helical Motions. The structure of the complex between the RING domain from c-Cbl and UbcH7 is an archetypal E2−E3 interaction and was used to develop a rough model of TRAF6-RD associated with its cognate E2 Ubc13 (Figure 6). Residues V81, T83, N115, L117, and F118 are involved in DSS binding, and the kinetics of this interaction are manifest as micro- to millisecond time scale chemical exchange and line shape perturbations upon changing the protein:DSS ratio. Interestingly, while the isolated RING domain from TRAF6 does not self-associate, these residues occur at the typical RING dimer interface, and this surface is different from that involved in the TRAF6−Ubc13 interaction. Of the residues involved in typical E2−E3 interactions, residues I98, R99, and D100 display micro- to millisecond time scale motions. While there are many enthalpic and entropic factors that determine the affinity of protein−protein and protein−ligand interactions, modulation of slow time scale motions observed for residues 98−100 (increases or decreases in flexibility) may be a general mechanism allowing precise adjustment of the affinities of E2−E3 interactions in achieving optimal substrate polyubiquitination. Specifically, quenching of these motions upon E2 binding may contribute unfavorably to the entropy of binding, and this may be an important mechanism for maintaining weak E2−E3 interactions, with fast kinetics, to allow for rapid transfer of ubiquitin to protein substrates bound to the E3 ligase. From a computational perspective, a recent 50 ns molecular dynamics study for receptor−ligand interactions led to the generalization that receptor flexibility contributes a large proportion of the compensating entropy/enthalpy terms of binding free energy (*60*). Quenching of chemical exchange has been observed experimentally through relaxation dispersion measurements for pheromone binding to major urinary protein (*61*). Ultimately, further experimental verification and longer time scale simulations will be necessary to test whether this generalization is applicable for slower time scale motions in E2−E3 ubiquitination systems.

ACKNOWLEDGMENT

We thank Lewis E. Kay for providing the {^{1}H}−^{15}N NOE pulse sequence and for helpful discussions regarding relaxation dispersion experiments, and the Canadian National High Field NMR Center (NANUC) for its assistance and use of the facilities. Operation of NANUC is supported by grants from the CIHR, the Natural Sciences and Engineering Research Council of Canada, and the University of Alberta.

REFERENCES

1. Bradley, J. R., and Pober, J. S. (2001) Tumor necrosis factor receptor-associated factors (TRAFs). *Oncogene 20*, 6482–6491.
2. Bodmer, J. L., Schneider, P., and Tschopp, J. (2002) The molecular architecture of the TNF superfamily. *Trends Biochem. Sci. 27*, 19–26.
3. Liu, Y. C. (2004) Ubiquitin ligases and the immune response. *Annu. Rev. Immunol. 22*, 81–127.
4. Watts, T. H. (2005) TNF/TNFR family members in costimulation of T cell responses. *Annu. Rev. Immunol. 23*, 23–68.
5. Kobayashi, T., Walsh, M. C., and Choi, Y. (2004) The role of TRAF6 in signal transduction and the immune response. *Microbes Infect. 6*, 1333–1338.
6. Chen, Z. J. (2005) Ubiquitin signalling in the NF-κB pathway. *Nat. Cell Biol. 7*, 758–765.
7. Ghosh, S., May, M. J., and Kopp, E. B. (1998) NF-κB and REL Proteins: Evolutionarily Conserved Mediators of Immune Responses. *Annu. Rev. Immunol. 16*, 225–260.
8. Ye, H., Arron, J. R., Lamothe, B., Cirilli, M., Kobayashi, T., Shevde, N. K., Segal, D., Dzivenu, O. K., Vologodskaia, M., Yim, M., Du, K., Singh, S., Pike, J. W., Darnay, B. G., Choi, Y., and Wu, H. (2002) Distinct molecular mechanism for initiating TRAF6 signalling. *Nature 418*, 443–447.
9. Regnier, C. H., Tomasetto, C., Moog-Lutz, C., Chenard, M. P., Wendling, C., Basset, P., and Rio, M. C. (1995) Presence of a new conserved domain in CART1, a novel member of the tumor necrosis factor receptor-associated protein family, which is expressed in breast carcinoma. *J. Biol. Chem. 270*, 25715–25721.
10. Mercier, P., Lewis, M. J., Hau, D. D., Saltibus, L. F., Xiao, W., and Spyracopoulos, L. (2007) Structure, interactions, and dynamics of the RING domain from human TRAF6. *Protein Sci. 16*, 602–614.
11. Deng, L., Wang, C., Spencer, E., Yang, L., Braun, A., You, J., Slaughter, C., Pickart, C., and Chen, Z. J. (2000) Activation of the IκB kinase complex by TRAF6 requires a dimeric ubiquitin-conjugating enzyme complex and a unique polyubiquitin chain. *Cell 103*, 351–361.
12. Lamothe, B., Besse, A., Campos, A. D., Webster, W. K., Wu, H., and Darnay, B. G. (2007) Site-specific Lys-63-linked tumor necrosis factor receptor-associated factor 6 auto-ubiquitination is a critical determinant of IκB kinase activation. *J. Biol. Chem. 282*, 4102–4112.
13. Petroski, M. D., Zhou, X., Dong, G., Daniel-Issakani, S., Payan, D. G., and Huang, J. (2007) Substrate modification with lysine 63-linked ubiquitin chains through the UBC13-UEV1A ubiquitin-conjugating enzyme. *J. Biol. Chem. 282*, 29936–29945.
14. He, L. S., Wu, X. L., Siegel, R., and Lipsky, P. E. (2006) TRAF6 regulates cell fate decisions by inducing caspase 8-dependent apoptosis and the activation of NF-κB. *J. Biol. Chem. 281*, 11235–11249.
15. Windheim, M., Peggie, M., and Cohen, P. (2008) Two different classes of E2 ubiquitin-conjugating enzymes are required for the mono-ubiquitination of proteins and elongation by polyubiquitin chains with a specific topology. *Biochem. J. 409*, 723–729.
16. Zheng, N., Wang, P., Jeffrey, P. D., and Pavletich, N. P. (2000) Structure of a c-Cbl-UbcH7 complex: RING domain function in ubiquitin-protein ligases. *Cell 102*, 533–539.
17. Vander Kooi, C. W., Ohi, M. D., Rosenberg, J. A., Oldham, M. L., Newcomer, M. E., Gould, K. L., and Chazin, W. J. (2006) The Prp19 U-box crystal structure suggests a common dimeric architecture for a class of oligomeric E3 ubiquitin ligases. *Biochemistry 45*, 121–130.
18. Knipscheer, P., and Sixma, T. K. (2007) Protein-protein interactions regulate Ubl conjugation. *Curr. Opin. Struct. Biol. 17*, 665–673.

19. Brzovic, P. S., Rajagopal, P., Hoyt, D. W., King, M. C., and Klevit, R. E. (2001) Structure of a BRCA1-BARD1 heterodimeric RING-RING complex. *Nat. Struct. Biol. 8*, 833–837.
20. Li, Z., Cao, R., Wang, M., Myers, M. P., Zhang, Y., and Xu, R. M. (2006) Structure of a Bmi-1-Ring1B polycomb group ubiquitin ligase complex. *J. Biol. Chem. 281*, 20643–20649.
21. Farrow, N. A., Muhandiram, R., Singer, A. U., Pascal, S. M., Kay, C. M., Gish, G., Shoelson, S. E., Pawson, T., Forman-Kay, J. D., and Kay, L. E. (1994) Backbone dynamics of a free and a phosphopeptide-complexed Src homology-2 domain studied by ^{15}N NMR Relaxation. *Biochemistry 33*, 5984–6003.
22. Kroenke, C. D., Loria, J. P., Lee, L. K., Rance, M., and Palmer, A. G. (1998) Longitudinal and transverse ^{1}H-^{15}N dipolar ^{15}N chemical shift anisotropy relaxation interference: Unambiguous determination of rotational diffusion tensors and chemical exchange effects in biological macromolecules. *J. Am. Chem. Soc. 120*, 7905–7915.
23. Tollinger, M., Skrynnikov, N. R., Mulder, F. A. A., Forman-Kay, J. D., and Kay, L. E. (2001) Slow dynamics in folded and unfolded states of an SH3 domain. *J. Am. Chem. Soc. 123*, 11341–11352.
24. Xu, X. P., and Case, D. A. (2001) Automated prediction of ^{15}N, ^{13}Cα, ^{13}Cβ and ^{13}C′ chemical shifts in proteins using a density functional database. *J. Biomol. NMR 21*, 321–333.
25. Xu, X. P., and Case, D. A. (2002) Probing multiple effects on ^{15}N, ^{13}Cα, ^{13}Cβ, and ^{13}C′ chemical shifts in peptides using density functional theory. *Biopolymers 65*, 408–423.
26. Moon, S., and Case, D. A. (2007) A new model for chemical shifts of amide hydrogens in proteins. *J. Biomol. NMR 38*, 139–150.
27. Smillie, L., and Nattriss, M. (1991) in *High-performance liquid chromatography of peptides and proteins: Separation, analysis, and conformation* (Mant, C. T., and Hodges, R. S., Eds.) pp 847−848, CRC Press, Boca Raton, FL.
28. Li, M. X., Spyracopoulos, L., and Sykes, B. D. (1999) Binding of cardiac troponin-I$_{147-163}$ induces a structural opening in human cardiac troponin-C. *Biochemistry 38*, 8289–8298.
29. Delaglio, F., Grzesiek, S., Vuister, G. W., Zhu, G., Pfeifer, J., and Bax, A. (1995) NMRPipe: A multidimensional spectral processing system based on UNIX Pipes. *J. Biomol. NMR 6*, 277–293.
30. Goddard, T. D., and Kneller, D. G. (2006) Sparky, University of California, San Francisco.
31. Loria, J. P., Rance, M., and Palmer, A. G. (1999) A relaxation-compensated Carr-Purcell-Meiboom-Gill sequence for characterizing chemical exchange by NMR spectroscopy. *J. Am. Chem. Soc. 121*, 2331–2332.
32. Mulder, F. A. A., Skrynnikov, N. R., Hon, B., Dahlquist, F. W., and Kay, L. E. (2001) Measurement of slow (μs-ms) time scale dynamics in protein side chains by ^{15}N relaxation dispersion NMR spectroscopy: Application to Asn and Gln residues in a cavity mutant of T4 lysozyme. *J. Am. Chem. Soc. 123*, 967–975.
33. Kovrigin, E. L., Kempf, J. G., Grey, M. J., and Loria, J. P. (2006) Faithful estimation of dynamics parameters from CPMG relaxation dispersion measurements. *J. Magn. Reson. 180*, 93–104.
34. Palmer, A. G., Kroenke, C. D., and Loria, J. P. (2001) Nuclear magnetic resonance methods for quantifying microsecond-to-millisecond motions in biological macromolecules. *Methods Enzymol. 339*, 204–238.
35. Mandel, A. M., Akke, M., and Palmer, A. G. (1995) Backbone dynamics of *Escherichia coli* ribonuclease HI: Correlations with structure and function in an active enzyme. *J. Mol. Biol. 246*, 144–163.
36. Spyracopoulos, L. (2006) A suite of Mathematica notebooks for the analysis of protein main chain ^{15}N NMR relaxation data. *J. Biomol. NMR 36*, 215–224.
37. d'Auvergne, E. J., and Gooley, P. R. (2003) The use of model selection in the model-free analysis of protein dynamics. *J. Biomol. NMR 25*, 25–39.
38. Horn, R. (1987) Statistical methods for model discrimination: Applications to gating kinetics and permeation of the acetylcholine-receptor channel. *Biophys. J. 51*, 255–263.
39. Carver, J. P., and Richards, R. E. (1972) General 2-site solution for chemical exchange produced dependence of T_2 upon Carr-Purcell pulse separation. *J. Magn. Reson. 6*, 89–105.
40. Markley, J. L., Bax, A., Arata, Y., Hilbers, C. W., Kaptein, R., Sykes, B. D., Wright, P. E., and Wüthrich, K. (1998) Recommendations for the presentation of NMR structures of proteins and nucleic acids (IUPAC Recommendations 1998). *Pure Appl. Chem. 70*, 117–142.
41. Murphy, J. M., Korzhnev, D. M., Ceccarelli, D. F., Briant, D. J., Zarrine-Afsar, A., Sicheri, F., Kay, L. E., and Pawson, T. (2007) Conformational instability of the MARK3 UBA domain compromises ubiquitin recognition and promotes interaction with the adjacent kinase domain. *Proc. Natl. Acad. Sci. U.S.A. 104*, 14336–14341.
42. Das, R., Abu-Abed, M., and Melacini, G. (2006) Mapping allostery through equilibrium perturbation NMR spectroscopy. *J. Am. Chem. Soc. 128*, 8406–8407.
43. Sugase, K., Dyson, H. J., and Wright, P. E. (2007) Mechanism of coupled folding and binding of an intrinsically disordered protein. *Nature 447*, 1021–1025.
44. Hill, R. B., Bracken, C., DeGrado, W. F., and Palmer, A. G. (2000) Molecular motions and protein folding: Characterization of the backbone dynamics and folding equilibrium of α_2D using ^{13}C NMR spin relaxation. *J. Am. Chem. Soc. 122*, 11610–11619.
45. Jee, J., Ishima, R., and Gronenborn, A. M. (2008) Characterization of specific protein association by ^{15}N CPMG relaxation dispersion NMR: The GB1(A34F) monomer-dimer equilibrium. *J. Phys. Chem. B 112*, 6008–6012.
46. Spyracopoulos, L., Lavigne, P., Crump, M. P., Gagné, S. M., Kay, C. M., and Sykes, B. D. (2001) Temperature dependence of dynamics and thermodynamics of the regulatory domain of human cardiac troponin C. *Biochemistry 40*, 12541–12551.
47. Hass, M. A. S., Hansen, D. F., Christensen, H. E. M., Led, J. J., and Kay, L. E. (2008) Characterization of conformational exchange of a histidine side chain: Protonation, rotamerization, and tautomerization of His61 in plastocyanin from *Anabaena variabilis*. *J. Am. Chem. Soc. 130*, 8460–8470.
48. Roehm, P. C., and Berg, J. M. (1997) Sequential metal binding by the RING finger domain of BRCA1. *Biochemistry 36*, 10240–10245.
49. Houben, K., Wasielewski, E., Dominguez, C., Kellenberger, E., Atkinson, R. A., Timmers, H. T., Kieffer, B., and Boelens, R. (2005) Dynamics and metal exchange properties of C4C4 RING domains from CNOT4 and the p44 subunit of TFIIH. *J. Mol. Biol. 349*, 621–637.
50. Kabsch, W., and Sander, C. (1983) Dictionary of protein secondary structure: Pattern recognition of hydrogen-bonded and geometrical features. *Biopolymers 22*, 2577–2637.
51. Millet, O., Loria, J. P., Kroenke, C. D., Pons, M., and Palmer, A. G. (2000) The static magnetic field dependence of chemical exchange linebroadening defines the NMR chemical shift time scale. *J. Am. Chem. Soc. 122*, 2867–2877.
52. Tjandra, N., Feller, S. E., Pastor, R. W., and Bax, A. (1995) Rotational diffusion anisotropy of human ubiquitin from ^{15}N NMR relaxation. *J. Am. Chem. Soc. 117*, 12562–12566.
53. Kentsis, A., Gordon, R. E., and Borden, K. L. B. (2002) Control of biochemical reactions through supramolecular RING domain self-assembly. *Proc. Natl. Acad. Sci. U.S.A. 99*, 15404–15409.
54. Pullen, S. S., Labadia, M. E., Ingraham, R. H., McWhirter, S. M., Everdeen, D. S., Alber, T., Crute, J. J., and Kehry, M. R. (1999) High-affinity interactions of tumor necrosis factor receptor-associated factors (TRAFs) and CD40 require TRAF trimerization and CD40 multimerization. *Biochemistry 38*, 10168–10177.
55. Wu, H., and Arron, J. R. (2003) TRAF6, a molecular bridge spanning adaptive immunity, innate immunity and osteoimmunology. *BioEssays 25*, 1096–1105.
56. Heldin, C. H. (1995) Dimerization of cell surface receptors in signal transduction. *Cell 80*, 213–223.
57. Xu, Z., Devlin, K. I., Ford, M. G., Nix, J. C., Qin, J., and Misra, S. (2006) Structure and interactions of the helical and U-box domains of CHIP, the C terminus of HSP70 interacting protein. *Biochemistry 45*, 4749–4759.
58. Kostic, M., Matt, T., Martinez-Yamout, M. A., Dyson, H. J., and Wright, P. E. (2006) Solution structure of the Hdm2 C2H2C4 RING, a domain critical for ubiquitination of p53. *J. Mol. Biol. 363*, 433–450.
59. Bellon, S. F., Rodgers, K. K., Schatz, D. G., Coleman, J. E., and Steitz, T. A. (1997) Crystal structure of the RAG1 dimerization domain reveals multiple zinc-binding motifs including a novel zinc binuclear cluster. *Nat. Struct. Biol. 4*, 586–591.
60. Baron, R., and McCammon, J. A. (2008) (Thermo)dynamic role of receptor flexibility, entropy, and motional correlation in protein-ligand binding. *ChemPhysChem 9*, 983–988.
61. Perazzolo, C., Verde, M., Homans, S. W., and Bodenhausen, G. (2007) Evidence of chemical exchange in recombinant Major Urinary Protein and quenching thereof upon pheromone binding. *J. Biomol. NMR 38*, 3–9.

BI800252X